Vol. 58: 235–246, 2014
doi: 10.3354/cr01193

CLIMATE RESEARCH
Clim Res

Published January 7

Warming patterns over the Tibetan Plateau and adjacent lowlands derived from elevation- and bias-corrected ERA-Interim data

Lars Gerlitz[1,*], Olaf Conrad[1], Axel Thomas[2], Jürgen Böhner[1]

[1]Institute of Geography, University of Hamburg, Bundesstraße 55, 20146 Hamburg, Germany
[2]GIS-Service GmbH, Am Graben 1, 55263 Wackernheim, Germany

ABSTRACT: For many ecological processes, near-surface temperature is one of the main controlling parameters. Since meteorological observations in high mountains are sparse, climate model data are frequently used. State of the art climate reanalysis products or general circulation models have a horizontal spatial resolution on the order of 50 × 50 km, i.e. far too coarse to represent the spatial variability of near-surface temperatures in mountain regions. Based on the assumption that elevation is the main factor determining the distribution of temperatures, we present a SAGA-GIS based approach for elevation and bias correction of climate model output data. Modeled temperature and geopotential height at different pressure levels were used to derive local temperature profiles by means of a polynomial regression approach. Atmospheric temperatures at surface level can then be derived from the regression equation. Compared with a simple elevation adjustment of ERA-Interim near-surface temperatures using an invariant lapse rate of 0.65°C per 100 m, the method showed good results, particularly in complex terrain. The method was used to generate high-resolution daily temperature fields for a target area in Central Asia for the period from 1989 onwards. Gridded trends of different temperature indices were calculated. For winter and spring, the highest temperature trends were detected in the high mountain regions. In summer, the calculated trend magnitudes were generally smaller. During the post-monsoon season, trends were more pronounced at low elevations. For the southern slopes of the Himalayan Arc and the valleys of the Tibetan Plateau, a significant decrease in frost days and an increase in growing degree days were detected.

KEY WORDS: Climate change · Geographical information systems · Climate regionalisation · Statistical downscaling

1. INTRODUCTION

Due to their complex ecosystems and their often marginalized economies, high mountain regions are considered to be among the most vulnerable environments in the context of climate change (Huber et al. 2005). Many studies, whether they were based on physical or statistical climate modeling applications or merely on the analysis of observations, have revealed that recent temperature trends at high elevations in general exceed the IPCC indicated global mean of 0.74°C over the last century (Shrestha et al. 1999, Liu & Chen 2000, Bolch et al. 2012).

Given that mountain regions are characterized by a huge variability of topoclimatic settings within short distances, they offer a variety of environments and often show a high rate of biodiversity (Körner 2004, Huber et al. 2005). This is particularly valid for the humid southern slopes of the Himalayas, which have been mentioned as one of 25 global biodiversity hotspots (Myers et al. 2000). Although the target area of our study is highly populated, there are still re-

*Corresponding author: lars.gerlitz@uni-hamburg.de

gions which are only negligibly influenced by human societies. In general, climatic changes due to greenhouse gas emissions are considered a serious risk to vulnerable mountain ecosystems (e.g. Pauli et al. 2007). Since near-surface temperature is among the main parameters controlling environmental processes — such as glacial, permafrost, or timberline dynamics — temporal and spatial high-resolution information about its mean values, its variability, and its rate of change is required for many ecological investigations and modeling approaches (Böhner & Lehmkuhl 2005, Yu et al. 2010, Bolch et al. 2012, Gao et. al. 2012).

The target area for our study covers the Tibetan Plateau, the main mountain ranges of High Asia, namely the Himalayan Arc, the Karakoram, and the Kunlun Mountains, as well as the adjacent lowlands of India and the Tarim Basin (Fig. 1). While the Ganges Brahmaputra Lowlands and the southern slopes of the Himalayan Mountains are characterized by a monsoonal climate with hyper-humid summer conditions, the Karakoram is influenced by both western circulation patterns and monsoonal currents (Böhner 2006). In contrast, the Tarim Basin is among the most continental areas of the world, influenced by dry and autochthonous climatic conditions (Böhner 2006). Thus the target area covers regions which differ not only in their specific topoclimatic settings, but also in their large-scale atmospheric characteristics.

Near-surface temperature and its spatial and seasonal trend distribution have been widely studied for the target area, mainly based on a sparse network of meteorological observations. Most studies estimate temporal temperature trends based on a linear regression approach. In general, statistically significant temperature trends have been detected, particularly during the winter season. Compared with the northern hemispheric mean temperature rise, the detected trends were higher over the Tibetan Plateau (You et al. 2010a) and in the Nepalese Himalayas (Shrestha et al. 1999). During recent decades, increasing warming trends for Tibet have been detected by Liu & Chen (2000) and Diodato et al. (2012). During the winter season, a distinct altitude dependency of warming trends for the Tibetan Plateau was detected by Liu & Chen (2000). Shrestha et al. (1999) found similar results for the high elevations of the Nepalese Himalayas. Based on principal component analysis using temperature records from 71 meteorological stations, You et al. (2010a) defined subregions of the Tibetan Plateau with similar warming trend characteristics. The strongest winter trends were found in the northeast subregion, while the southeast of the Tibetan Plateau showed the lowest response to global warming. Based on dynamical downscaling using the hydrostatic regional climate model REMO, Mannig et al. (2013) concluded that the Central Asian deserts (e.g. the Tarim Basin) are affected by intensified summer warming. Based on the monthly mean temperature records from 24 meteorological stations, Zhang et al. (2010) found the highest temperature trends for the Tarim Basin in autumn, while no statistically significant trend could be detected during the winter season.

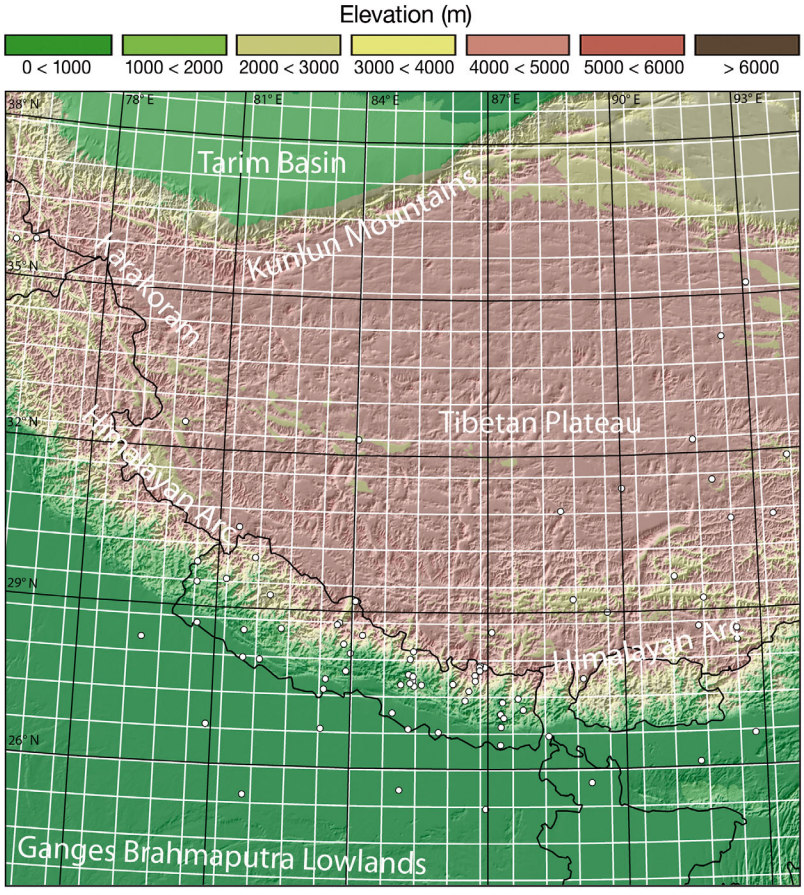

Fig. 1. Target area and its main geomorphological features. The points indicate the locations of available meteorological observations, and the white grid shows the spatial resolution of state of the art reanalysis products (0.7° grid)

You et al. (2008) showed that minimum temperature trends over the Tibetan Plateau are larger compared with mean or maximum values. For the lowlands of India, Jain et al. (2013) and Arora et al. (2005) detected positive trends, particularly for maximum temperatures during the post-monsoon season. For minimum temperatures, decreasing trends were found at some stations.

Frauenfeld et al. (2005) found significant trends of observed monthly mean temperatures for the Tibetan Plateau, particularly for the northeastern and the southeastern part for the period 1958–2000. Since those trends could not be confirmed with low-resolution ERA-40 reanalysis data, they suggested that the observed changes are more likely to be due to land use change. However, You et al. (2010b) found significant warming trends in the ERA-40 reanalysis data for the Tibetan Plateau, but also demonstrated that those trends are underestimated compared with observations. Pepin & Seidel (2005) argued that observed temperature trends are sensitive to the specific topographic situation and hence trends of reanalysis products might be unrealistically small for mountain environments. Gaffen et al. (2000) detected significant changes in lower tropospheric lapse rates for the period 1979–1997, which might result in a spatial differentiation of near-surface temperature trends in complex terrain.

Since meteorological stations are sparsely distributed, particularly in the western part of the Tibetan Plateau (Fig. 1), and most stations are located in valleys, the spatial variability and trends of near-surface temperatures in the highly textured target area are not sufficiently represented by observations. Facing the growing demand for spatial and temporal high-resolution temperature data, we present a GIS-based approach to increase the spatial resolution of daily ERA-Interim reanalysis data by means of elevation and bias correction. This approach considers the current stratification of the atmosphere by processing temperature values on several ERA-Interim pressure levels. The results were compared with the low-resolution ERA-Interim 2 m temperature- and the elevation-adjusted 2 m temperature based on a linear lapse rate of 0.65°C per 100 m. Subsequently, several temperature indices and their temporal trends were estimated on a 1 km^2 grid covering the whole area of investigation, to identify the spatial distribution of warming for different seasons. The results were successfully validated using available observations.

2. DATA AND METHODS

For recent decades, gridded global reanalysis products are considered as the best estimates of large-scale meteorological variables, since they merge modeling results with *in situ* observations and remote sensing data using a data assimilation system. For this study, we used the ERA-Interim reanalysis, which is currently developed at the European Centre for Medium-Range Weather Forecasts (ECMWF), and covers the period from 1979 onwards. The ECMWF provides 6-hourly estimates of meteorological variables on a spectral T255 resolution (0.7° Lat./Long.) for 60 pressure levels ranging from sea level to the upper stratosphere. Compared with the anterior reanalysis generation ERA-40, covering the period 1957–2002, ERA-Interim stands out due to its improved representation of the hydrological cycle and stratospheric circulation and an advanced 4D data assimilation system (Berrisford et al. 2009, Dee et al. 2011)

Wang & Zeng (2012) evaluated the skills of different reanalysis products for the Tibetan Plateau with 63 independent meteorological station records, and concluded that ERA-Interim is able to capture the large-scale variability of near-surface temperatures in the target area. Bao & Zhang (2013) compared temperature profiles of various reanalysis products with 3000 independent sounding observations during a short monitoring period in summer 1992. ERA-Interim was found to have the lowest bias below the 250 hPa level. Compared with the NCEP-reanalysis, You et al. (2010b) showed that near-surface temperature trends in the target area are better represented by the ERA-40 reanalysis.

For the presented approach we used free atmosphere temperature and geopotential values for the levels 1000, 925, 850, 700, 600, 500, 300, and 200 hPa. These cover the relief altitudes in the target area ranging from almost sea level in the lowlands of India up to more than 8000 m a.s.l. in the high Himalayas (Fig. 1). Furthermore, the main weather-relevant large-scale atmospheric processes, such as the low level monsoonal current or the upper tropospheric jet stream, fall within this altitudinal range. Geopotential height was calculated by dividing geopotential values by gravity. Daily means of large-scale atmospheric variables were calculated by averaging the 4 daily reanalysis fields.

For high-resolution digital representation of orography we used the freely available SRTM Digital Elevation Model (DEM), published by the CGIAR-Consortium for Spatial Information (http://srtm.

csi.cgiar.org), covering the entire globe between 60° N and 58° S with a cell size of 90 m (Farr et al. 2007, Reuter et al. 2007).

For bias correction and validation purposes, we used time series of observed daily mean temperature for 78 stations, most of them covering the period 1989–2010. For the Tibetan Plateau and the lowlands of India, the available observations were freely obtained from the Global Summary of the Day Project of the National Climatic Data Center and the National Oceanic and Atmospheric Administration. For Nepal, time series of 40 stations were provided by the Department of Hydrology and Meteorology/ Ministry of Science, Technology and Environment (DHM) in Kathmandu. An additional data set with observed records of 8 stations in high mountain environments at altitudes up to 8000 m a.s.l. was provided by the Ev-K2-CNR-project (www.evk2cnr.org). The observations provided by the DHM and the Ev-K2-CNR-project have not been published and thus have not been assimilated in the ERA-reanalysis (R. Karki and P. Stocchi pers. comm.). Hence most of the stations used for this study can be considered statistically independent.

The available temperature records were quality proofed using the relative residual-analytic approach proposed by Böhner (1996). For every individual temperature record T(t), 3 stations were identified, whose time series showed the highest correlation with the selected record. These were subsequently used to estimate T(t) based on a linear regression approach. The analysis of residuals (estimation minus observation) allows the identification of sudden changes and unlikely anomalies. Temperature records with obvious inhomogeneities were rejected, as were single values with unlikely residuals; as a threshold value we chose 3× the standard deviation of all residuals.

2.1. Correction of elevation

Since most meteorological stations in the target area are situated in valleys with elevations below the correspondent ERA-Interim grid cell, observed local temperatures tend to be warmer than the large-scale reanalysis results. This is particularly valid for high mountain regions with structured terrain.

Gao et al. (2012) compared different elevation-correction methods for ERA-Interim reanalysis data in the European Alps and concluded that methods based on a constant lapse rate derived from literature (such as the often cited environmental lapse rate of 0.65°C per 100 m) tend to fail in high mountain environments. Minder et al. (2010) and Pepin & Losleben (2002) illustrated that temperature lapse rates in mountains are highly dependent on the synoptic situation and thus cannot be considered invariant. Methods which consider the current stratification of the atmosphere derived from ERA-Interim intern temperature profiles seem to be promising alternatives. These allow e.g. the reproduction of inverse atmospheric temperature profiles, which occur mainly during the winter season.

Based on that principle, we used the above mentioned ERA-Interim fields of temperature and geopotential height to calculate daily gridded near-surface temperature values with high spatial resolution. The reanalysis data and the SRTM DEM were projected to a UTM 45 coordinate system, which is almost distortion-free for the target area, and resampled to a 1 km^2 spatial resolution. For refining the ERA-Interim pressure fields, we used spline interpolation, and the aggregation of the DEM was performed using a weighted average algorithm (Conrad 2006).

For each grid cell, the ERA-Interim internal temperature profile was calculated as a third-order curvilinear (polynomial) function of altitude. We assume that the spatial and temporal variability of near-surface temperature in complex terrain can be adequately modeled by considering the free-air lapse rates derived from ERA-Interim pressure levels for every time step and grid cell. A third-order polynomial fit allows a maximum of 2 local temperature extreme values, and hence can sufficiently represent typical temperature profiles (such as atmospheric inversions) in mountain areas:

$$t(x_i) = a_1 + a_2 \times x_i + a_3 \times x_i^2 + a_4 \times x_i^3 + \varepsilon_i \quad (1)$$

where a_i represent the cefficients of the polynominal function, x_i is the altitude in meters, $t(x_i)$ is the temperature at altitude x_i, and ε_i describes the residual of the regression.

Using matrix algebra, this term can be noted as:

$$\vec{T} = \vec{a} \times \vec{X} + \vec{\varepsilon} \quad (2)$$

where $\vec{T}$ is the matrix of temperature values at the ERA-Interim pressure levels and $\vec{X}$ is the corresponding matrix with geopotential height values. $\vec{a}$ describes the polynomial coefficients and $\vec{\varepsilon}$ indicates the residuals of the regression model.

Methodically, a polynomial fit can be treated as a multivariate linear regression function, using the independent variable and its polynomial modifications as predictors. On condition that the curvilinear regression function should minimize the sum of squared residuals, the vector of polynomial coefficients can be calculated as:

$$\vec{a} = (\vec{X}^T \vec{X})^{-1} \vec{X}^T \vec{T} \quad (3)$$

where X^T is the transpose of X.

The ERA-Interim temperature profiles were found to be well represented by the curvilinear fit. The coefficient of determination of the polynomial regression function did not fall below 95% at any grid cell or time step.

In conclusion, the free atmospheric temperature at surface elevation, which is given by the SRTM DEM, can be calculated using Eq. (1). This elevation-correction approach for gridded climate model output data with limited spatial resolution has been developed as a complete tool for the free and open source software SAGA-GIS in version 2.1. (www.saga-gis.org).

2.2. Correction of bias

The elevation-corrected daily values of temperature were subsequently compared with available observations. Since the modeling approach generates free atmospheric values at surface level without accounting for surface energy balance processes, such as solar insolation or latent heat transfer, residuals are still remarkably high. However, their analysis reveals temporal and spatial principles, which enable the implementation of a bias-correction approach.

For all stations, we identified a seasonal cycle of residuals. During winter season (DJF), a warm bias of the elevation-corrected ERA-Interim data (negative residuals; Fig. 2) was found for almost all meteorological stations in the target area, although the bias was less pronounced on the Tibetan Plateau compared to the rest of the target area. For the summer season (JJA), a cold bias (positive residuals) is characteristic. In particular, the stations on the Tibetan Plateau — such as Shiquanhe (32.50° N, 80.083° E) in the far west and Xainza (30.95° N, 88.633° E) on the Central Plateau — show a sinus like seasonal cycle of residuals (see Fig. 2). These were found to be strongly correlated ($r > 0.5$) with high-resolution estimates of incoming solar radiation, calculated using the methods of Böhner & Antoni (2009). Residuals tend to be positive throughout the year with maximum values of up to +5°C during the summer season, which is thought to be due to the high rates of solar insolation at high elevations.

For the stations in the Himalayan Arc and in the lowlands of India, the correlation between solar radiation and residuals was not statistically significant ($\alpha = 0.95$). Particularly in the eastern part of the Indus Brahmaputra Lowlands, the residuals show a secondary peak during February and March (see Station Patna in Fig. 2).

For the adjustment of those regularly occurring residuals, multi-year monthly mean values were calculated for every station and then spatially interpolated using spline interpolation. The monthly means of residuals were found to be invariant and did not show any trends. The interannual variability of monthly residual means was found to be low with standard deviations below ±1°C for all stations and seasons. Fig. 3 shows the spatial distribution of residuals for the selected months of January, April, July, and October. The winter season is dominated by negative residuals. During spring, when radiation values rise, positive residuals occur mainly on the Tibetan Plateau. In summer, the whole target area shows positive residuals, but maximum values remain at the high elevations.

Beside this regular seasonal cycle of residuals, which seems to be persistent and did not show statistically significant trends ($\alpha = 0.95$) at any station, a non-predictable high frequency variability of residuals with lower magnitude is characteristic for all stations (see Fig. 2). We assume that these temperature fluctuations are due to mesoscale or local circulation patterns and hence cannot be captured by Global Circulation Models or reanalysis products with limited spatial resolution. For the explanation of those high-frequency temperature fluctuations, advanced dynamical and statistical downscaling methods are necessary (Böhner 2006, Ji & Kang 2013).

The results of the presented approach were evaluated using available observations. Additionally, we compared the results with the low-resolution ERA-Interim 2 m temperature and the elevation-adjusted 2 m temperature based on a constant lapse rate of 0.65°C per 100 m.

The presented approach explains approximately 60% of the RMSE of the low-resolution ERA-Interim 2 m temperature in the highly structured target area, and outperforms the simple elevation adjustment based on a constant lapse rate (Table 1). In the mountainous regions with elevations ranging from 1000 to above 4000 m a.s.l., the RMSE of the reanalysis data decreased respectively by up to 80% (Table 1). The RMSE of modeled daily mean temperature values dropped below 2°C for almost all stations, when the current stratification of the atmosphere is considered. Elevation-adjusted temperatures based on a constant lapse rate showed explicitly higher errors with characteristic values between 2 and 6°C (Table 1 and see Table S1 in the supplement at www.int-res.com/articles/suppl/c058p235_supp.pdf). Particularly for

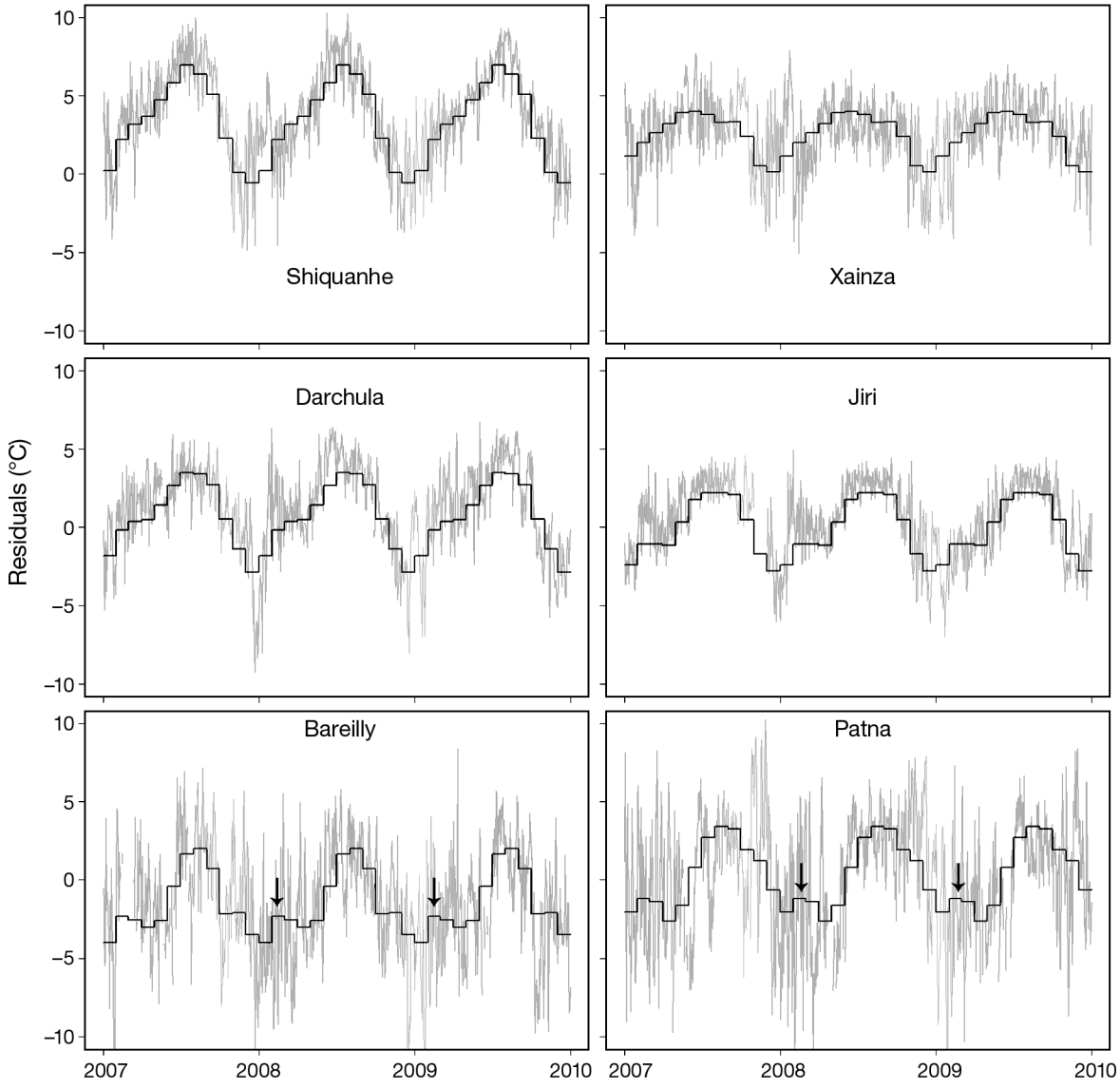

Fig. 2. Annual cycle of residuals (observed minus modeled temperatures) for selected stations: Shiquanhe (32.5° N, 80.083° E, Western Plateau), Xainza (30.95° N, 88.633° E, Central Plateau), Darchula (29.849° N, 80.542° E, Western Himalayas), Jiri (27.633° N, 86.233° E, Eastern Himalayas), Bareilly (28.367° N, 79.40° E, Western Lowlands), and Patna (25.591° N, 85.088° E, Eastern Lowlands). Black line: (invariant) multi-year monthly mean of residuals; ticks on the *x*-axis: beginning of labeled year; arrows: secondary maximum of residuals for stations in the Indian lowlands

the high mountain stations where near-surface temperatures are mainly influenced by large-scale atmospheric patterns (Gao et al. 2012), the added value of the approach was comparatively high, with decreasing RMSE values of up to 94 % at Colle Sud (27.96° N, 86.93° E) at 8000 m a.s.l. (Table S1). In the lowlands of India with elevations below 500 m and on the Tibetan Plateau between 4500 and 5000 m a.s.l., no added value of the approach could be identified. The topography of those regions is less complex and hence presumably better represented by the ERA-Interim reanalysis. RMSE values of the elevation and bias-corrected temperature data remained in the same dimension.

2.3. Calculation of temperature indices and trends

Based on the elevation- and bias-adjustment approach, gridded daily temperature fields were generated for the period 1989–2010. The term 'trend' in this context denotes a temporal linear trend, derived with the help of a linear regression; values are positive if not stated otherwise. Subsequently, we calcu-

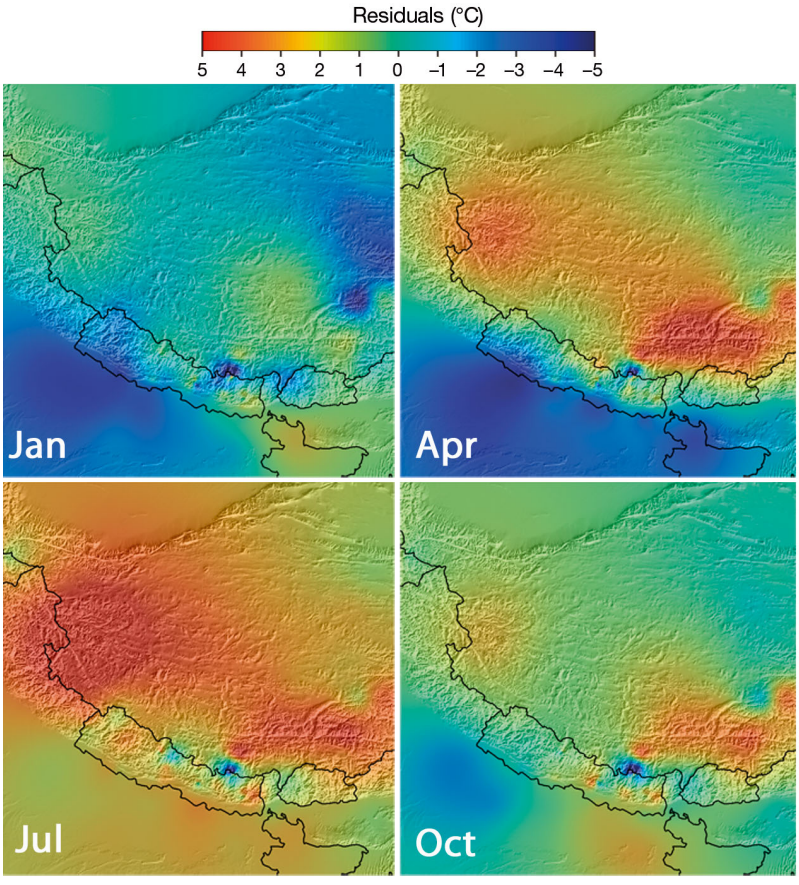

Fig. 3. Spatial distribution of residuals for the selected months of January, April, July, and October based on spline-interpolation of monthly means

lated average, minimum, and maximum values of daily mean temperatures. Furthermore, accumulative temperature indices like the annual number of frost days with daily mean temperatures below 0°C and the number of tropical days with temperatures above 25°C were calculated. The number of growing degree days was computed as the time span between the first period of 5 d with daily mean temperatures above 5°C after winter and the last period of 5 d with more than 5°C after summer (Alley et al. 2007)

Gridded linear trends of mean, minimum, and maximum temperature were calculated for every month using a least square fit. For the accumulative temperature indices, annual trends were calculated. Trends were considered significant when the Pearson correlation of time (being the independent variable) with temperature values was significant at the 95% level. The test statistic t_p was calculated to $t_p = r \times \sqrt{n-2} / \sqrt{1-r^2}$ and compared with the critical value of the t-distribution. n represents the number of years, r is the correlation coefficient of the specfic parameter with time, r^2 is the percentage of variance explained by the linear trend (von Storch & Zwiers 2001).

Significant trends of the elevation- and bias-corrected ERA-Interim data were compared with trends of the low-resolution 2 m temperature and evaluated with available observations. It must be noted that since the correction of bias is invariant, the computed temperature trends only depend on changes in the ERA-Interim intern temperature profiles.

Table 1. RMSE of ERA-Interim 2 m temperature (ERA 2 m), the linear elevation-adjusted data set (ERA 2 m cor), and the elevation- and bias-corrected data set (ERA bias cor) for different altitude bands

Altitude band (m)	n	ERA 2 m		ERA 2 m cor		ERA bias cor	
		(°C)	(%)	(°C)	(%)	(°C)	(%)
All stations	78	5.21	100	2.96	56.81	2.09	40.12
<500	20	2.86	100	2.17	75.87	3.06	106.99
500–1000	3	5.78	100	3.23	55.88	2.28	39.45
1000–1500	10	5.38	100	2.42	44.98	1.54	28.62
1500–2000	7	6.02	100	3.53	58.64	1.36	22.59
2000–2500	6	4.34	100	3.14	72.35	1.63	37.56
2500–3000	5	4.26	100	3.19	74.88	1.85	43.43
3000–3500	1	13.14	100	4.33	32.95	2.01	15.30
3500–4000	8	6.01	100	2.68	44.59	1.83	30.45
4000–4500	7	4.84	100	2.98	61.57	1.92	39.67
4500–5000	8	1.79	100	2.91	162.57	1.95	108.94
>5000	3	23.39	100	8.03	34.33	1.61	6.88

3. RESULTS

In general, the spatial and seasonal distribution of trends was consistent with observed values. As shown in Fig. 4, significant trends of the ERA-Interim 2 m temperature (left) as well as trends of the elevation- and bias-corrected data set (right) are of comparable dimension to observed values, although the low-resolution ERA-Interim 2 m data set tends to underestimate the temperature trends in some cases.

The correlations of ERA-Interim 2 m trends with observed temperature

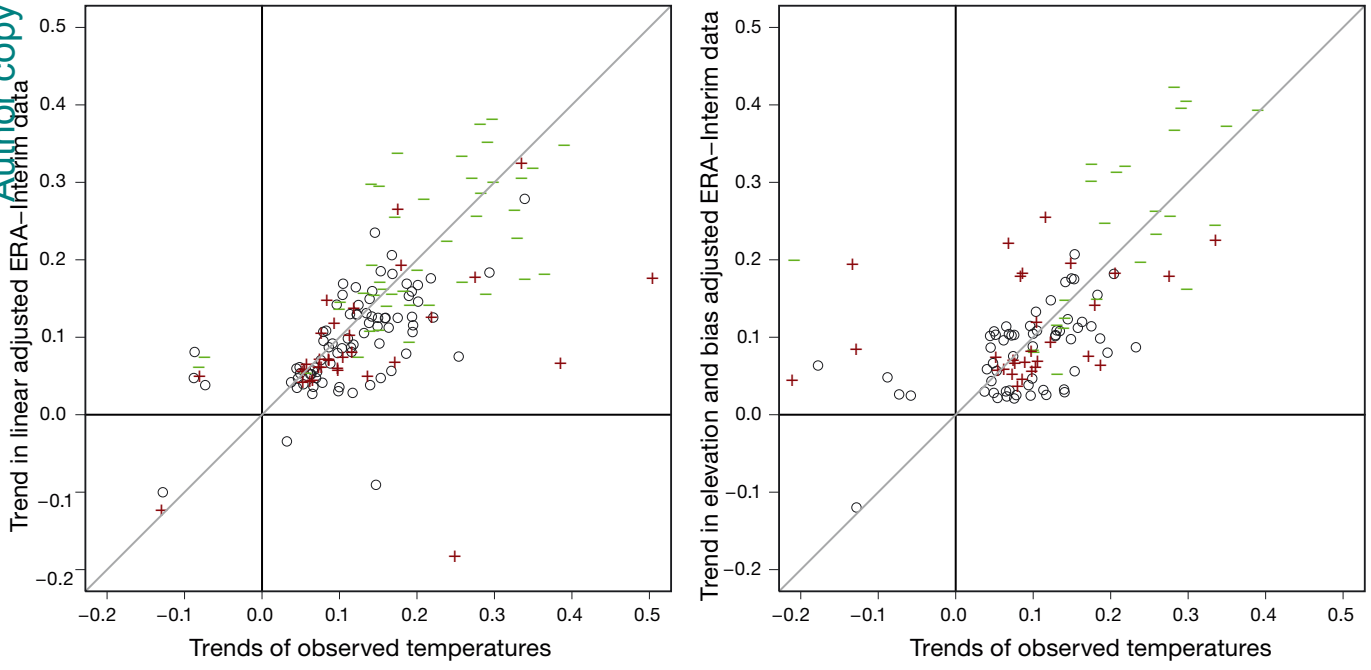

Fig. 4. Comparison of modeled and observed significant trends for the low-resolution ERA-Interim 2 m temperature (left) and the elevation- and bias-adjusted temperature (right). Circles: trend of mean monthly temperature; '+' and '−': trends of maximum and minimum temperatures, respectively

trends amount to 0.56, 0.69, and 0.66 for mean, minimum, and maximum monthly temperature, respectively. For the elevation- and bias-adjusted data set, the correlations slightly increase to 0.79, 0.65, and 0.77. The improved representation of trends may indicate a change of lapse rates in the target area (as proposed by Gaffen et al. 2000), which can be better captured by considering the temperature on different ERA-Interim pressure levels, although a more detailed analysis of lapse rate change in High Asia is beyond the scope of this study.

Based on the elevation- and bias-adjusted data set and on observed temperature records, the investigation of the spatial and seasonal distribution of near-surface temperature trends for the target area revealed the following results. During the winter season, the highest trends of monthly mean temperatures were detected for the northeastern part of the Tibetan Plateau. This is mainly due to increasing minimum temperatures of up to 1°C decade^{-1} (see Fig. 6), and is in concordance with high trend values at the Chinese stations Wudaoliang (35.22° N, 93.08° E) and Tuatuohe (34.217° N, 92.433° E) (not shown). A second maximum of gridded temperature trends was indicated for the Ganges Brahmaputra Lowlands, but could not be validated with available observations (see Station Patna in Fig. 5).

During the pre-monsoon season (MAM), a warming trend maximum of more than 1°C decade^{-1} was found for the high mountain environments of the Tibetan Plateau, particularly the western part, and the adjacent mountain ranges. This can be confirmed e.g. with observations of Stations Shiquanhe and Darchula (Fig. 5). Again the increase of minimum temperatures is most pronounced, although the lowlands of India and the Tarim Depression show comparatively high trends of maximum temperatures in April (Fig. 6). During May, both observed and modeled mean temperatures show a decreasing trend, particularly in northeast India. We assume that this is caused by intrinsic climate variability. In general, the trends of monthly mean temperatures in the lowlands of India are small and not statistically significant during the spring season. The altitude dependency of warming trends in winter and spring could be reconstructed.

During summer, warming trends are lower in the entire target area. Merely the Tarim Basin and the eastern part of the Indian lowlands show significant mean temperature trends of approximately 0.6°C decade^{-1}. Warming trends in the high mountain environments are not pronounced; however, in the northeastern part of the Tibetan Plateau, we detected increasing minimum temperatures.

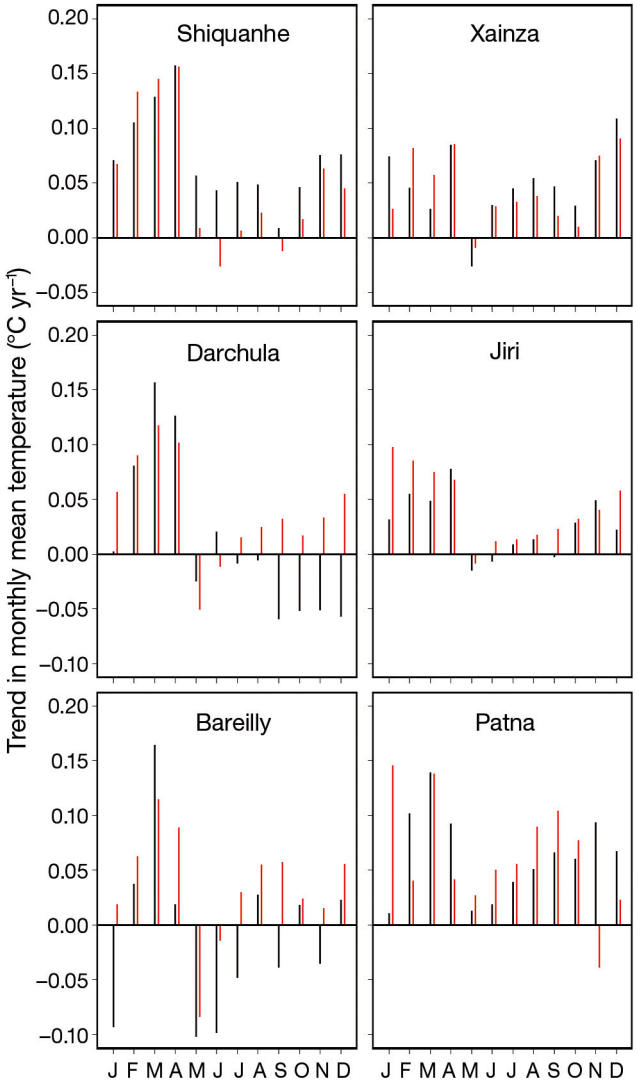

Fig. 5. Trends in observed (black) and modeled (red) mean monthly temperature for selected stations: Shiquanhe, Xainza, Darchula, Jiri, Bareilly, and Patna (coordinates for all stations are given in Fig. 2)

The post-monsoon season (SON) is likewise characterized by increased warming trends in the lowlands (see e.g. Station Patna in Fig. 5) with maximum values in the Tarim Basin of more than 1°C decade^{-1} (Fig. 6).

The trends of accumulative temperature indices (Fig. 7) are characteristic for specific regions in the target area, respectively. Particularly for the southern slopes of the Himalayan Range, the Kunlun Mountains, and the valleys of the Tibetan Plateau with elevations between 3000 and 5000 m a.s.l., a statistically significant decrease of annual frost days was detected. Especially in the Nepalese Himalayas, the trends amount to approximately −17 d decade^{-1}. This might be of special interest for the analysis of permafrost dynamics in the high mountain environments of the target area. Increases in the number of tropical days with mean daily temperatures above 25°C were monitored in the eastern parts of the Indian lowlands as well as in the west of the Tarim Basin. Likewise, the southern slopes of the Himalayan Arc show significant increasing trends in the number of tropical days at altitudes below 1500 m.

For the valleys of the Tibetan Plateau, the Tarim Basin, and in particular for the southern slopes of the Himalayas (at elevations between 2000 and 3500 m a.s.l.), an enhanced trend of growing degree days with values of up to 12 d decade^{-1} was detected. Given that the timberline of the Himalayas falls within this altitudinal range, the extension of the vegetation period will most likely alter the growing conditions at the treeline ecotone.

4. SUMMARY AND OUTLOOK

For many ecological studies, local information about surface air temperature, its variability, and trends are required. Particularly in high mountain regions, where the network of meteorological observations is sparse, such information is often not available. Climate modeling results can bridge this gap, but often have a large bias due to the limited spatial resolution of the modeling domain. Especially in mountains, the spatial variability of near-surface temperature cannot be captured by state of the art climate models. Since elevation is the main controlling parameter for the variability of near-surface temperature in complex terrain, the presented approach of elevation and bias correction can clearly improve the quality of climate model output data. In less complex terrain, the added value of the approach was found to be less pronounced. The methods are completely implemented in the free and open source software SAGA-GIS, and hence are freely available to the broad community dealing with climate-related problems.

By means of the presented methods, a data set of daily high-resolution near-surface temperatures was generated for a target area, covering the Tibetan Plateau, the main mountain ranges of Central Asia, and the adjacent lowlands for the period 1989–2010. It was shown that the ERA-Interim reanalysis is able to capture the large-scale temperature variability and trends in the target area. Using altitude and bias correction, the RMSE of the reanalysis data could be reduced by up to 80%, particularly in the high mountain regions. Therefore, the presented approach clearly

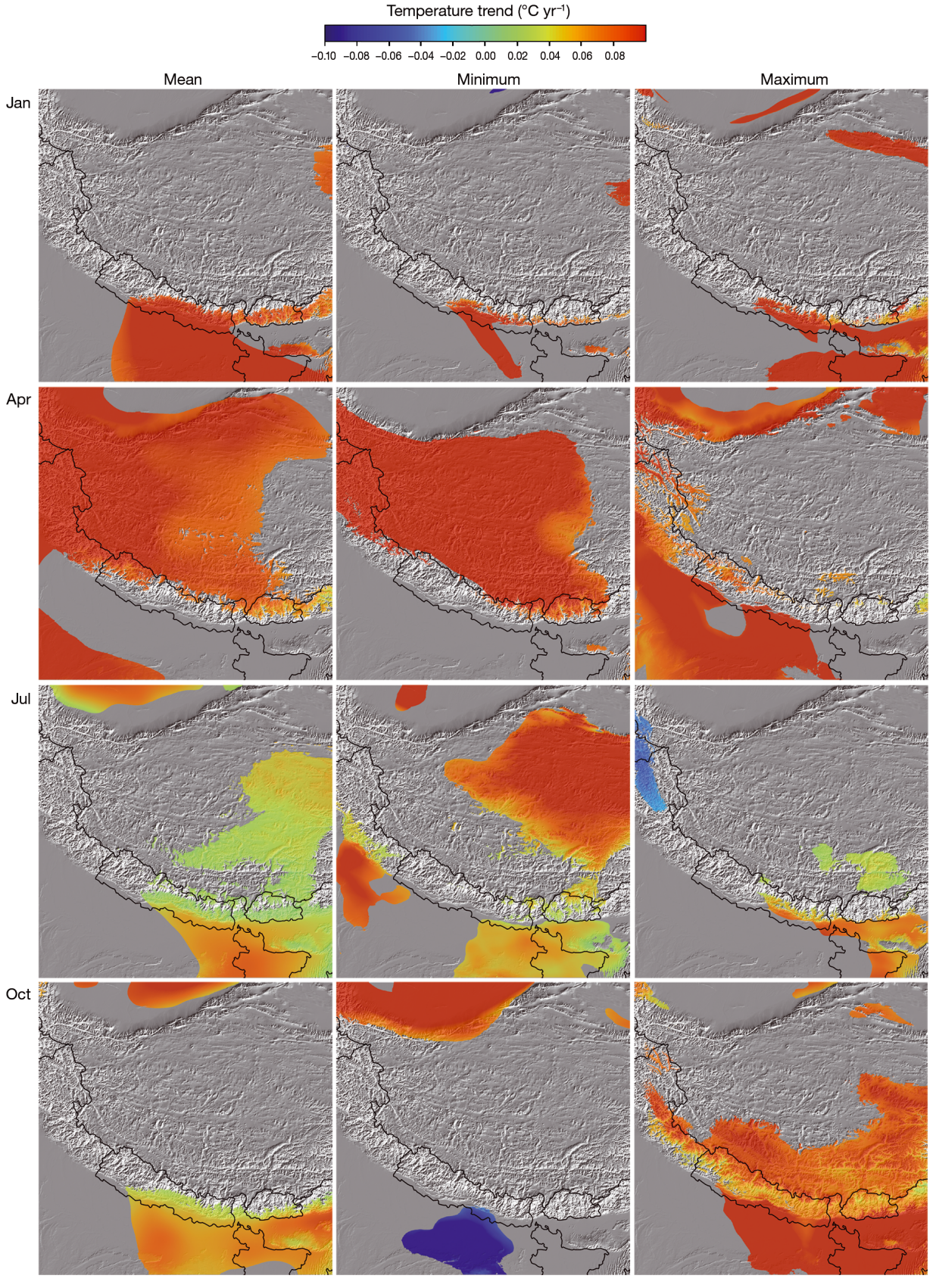

Fig. 6. Monthly mean (left), minimum (middle), and maximum (right) temperature trends for the selected months of January, April, July, and October (from top to bottom). Trends are only shown when significant at the 95% level

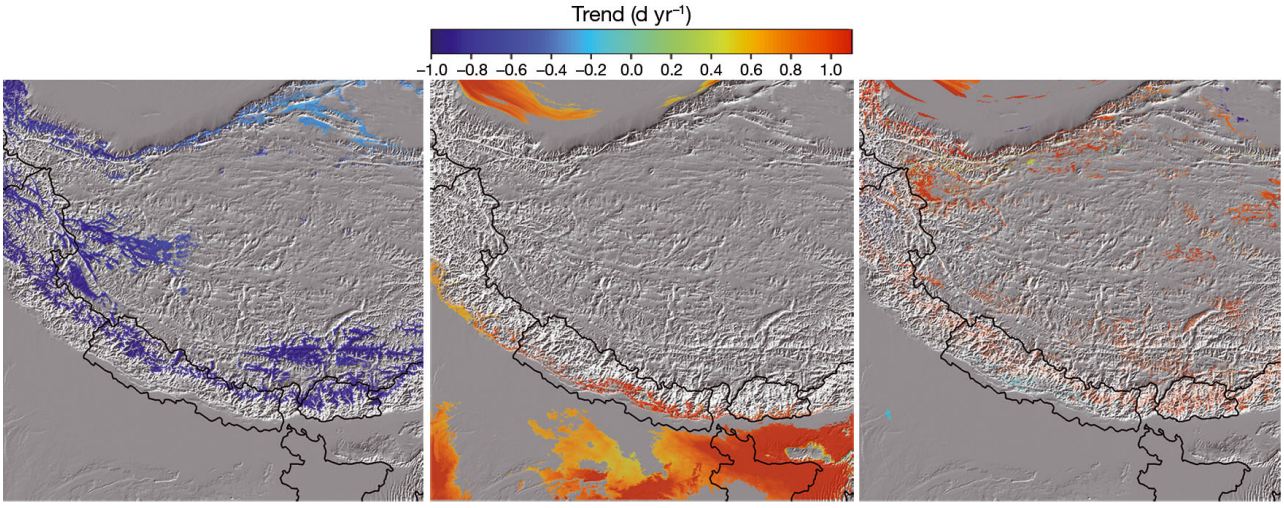

Fig. 7. Trends of frost days (left), tropical days (middle), and growing degree days (right). Values are in d yr^{-1}. Trends are only shown when significant at the 95% level

outperforms simple elevation adjustment methods based on an invariant lapse rate. Nevertheless, high-frequency, non-predictable residuals remain, which are suggested to be due to mesoscale and local circulation patterns. For their explanation, advanced statistical or dynamical downscaling methods need to be developed, which is a key aspect of our current research.

Based on the elevation- and bias-adjusted data set, the spatial and seasonal distribution of temperature trends in the target area was investigated and evaluated using available observations. The largest trend magnitudes were found during winter and the pre-monsoon season, particularly in the high elevations of the Tibetan Plateau and the bordering mountain ranges. During summer and the post-monsoon season, the detected trends are in general smaller with maximum values in the lowlands of India and the Tarim Basin.

Acknowledgements. The ERA-Interim reanalysis fields were freely provided by the ECMWF. We appreciate the supply of daily meteorological observations by the Department of Hydrology and Meteorology (Kathmandu, Nepal), the Ev-K2-CNR-Project (Bergamo, Italy), and the Global Summary of the Day Project.

LITERATURE CITED

Alley R, Berntsen T, Bindoff NL, Chen Z and others (2007) IPCC 2007: summary for policymakers. In: Solomon S, Qin D, Manning M, Chen Z and others (eds) Climate change 2007: the physical science basis. Contribution of Working Group I to the Fourth Assessment Report of the Intergovernmental Panel on Climate Change. Cambridge University Press, Cambridge, p 1–18

Arora M, Goel NK, Singh P (2005) Evaluation of temperature trends over India / Evaluation de tendances de température en Inde. Hydrol Sci J 50:1–93

Bao X, Zhang F (2013) Evaluation of NCEP/CFSR, NCEP/NCAR, ERA-Interim and ERA-40 Reanalysis datasets against independent sounding observations over the Tibetan Plateau. J Clim 26:206–214

Berrisford P, Dee D, Fielding K, Fuentes M, Kallberg P, Kobayashi S, Uppala S (2009) The ERA-Interim Archive. ERA Rep Ser 1. ECMWF, Shinfield Park

Böhner J (1996) Säkulare Klimaschwankungen und rezente Klimatrends Zentral- und Hochasiens. Goltze, Göttingen

Böhner J (2006) General climatic controls and topoclimatic variations in Central and High Asia. Boreas 35:279–295

Böhner J, Antonić O (2009) Land-surface parameters specific to topo-climatology. In: Hengl T, Reuter HI (ed) Developments in soil science, Vol 33. Elsevier, Amsterdam, p 195–226

Böhner J, Lehmkuhl F (2005) Environmental change modelling for Central and High Asia: Pleistocene, present and future scenarios. Boreas 34:220–231

Bolch T, Kulkarni A, Kääb A, Huggel C and others (2012) The state and fate of Himalayan glaciers. Science 336:310–314

Conrad O (2006) SAGA-Entwurf, Funktionsumfang und Anwendung eines Systems für automatisierte geowissenschaftliche Analysen. Niedersächsische Staats- und Universitätsbibliothek, Göttingen

Dee DP, Uppala SM, Simmons AJ, Berrisford P and others (2011) The ERA-Interim reanalysis: configuration and performance of the data assimilation system. QJR Meteorol Soc 137:553–597

Diodato N, Bellocchi G, Tartari G (2012) How do Himalayan areas respond to global warming? Int J Climatol 32: 975–982

Farr TG, Rosen PA, Caro E, Crippen R and others (2007) The shuttle radar topography mission. Rev Geophys 45: RG2004, doi:10.1029/2005RG000183

Frauenfeld OW, Zhang T, Serreze MC (2005) Climate change and variability using European Centre for Medium-Range Weather Forecasts reanalysis (ERA-40) temperatures on the Tibetan Plateau. J Geophys Res 110:D02101, doi:10.1029/2004JD005230

Gaffen DJ, Santer BD, Boyle JS, Christy JR, Graham NE,

Ross RJ (2000) Multidecadal changes in the vertical temperature structure of the tropical troposphere. Science 287:1242–1245

Gao L, Bernhardt M, Schulz K (2012) Downscaling ERA-Interim temperature data in complex terrain. Hydrol Earth Syst Sci Discuss 9:5931–5953

Huber UM, Bugmann HKM, Reasoner MA (2005) Global change and mountain regions: an overview of current knowledge. Springer, Dordrecht

Jain SK, Kumar V, Saharia M (2013) Analysis of rainfall and temperature trends in northeast India. Int J Climatol 33: 968–978

Ji Z, Kang S (2013) Double-nested dynamical downscaling experiments over the Tibetan Plateau and their projection of climate change under two RCP scenarios. J Atmos Sci 70:1278–1290

Körner C (2004) Mountain biodiversity, its causes and function. Ambio 13(Special No):11–17

Liu X, Chen B (2000) Climatic warming in the Tibetan Plateau during recent decades. Int J Climatol 20:1729–1742

Mannig B, Müller M, Starke E, Merkenschlager C and others (2013) Dynamical downscaling of climate change in Central Asia. Global Planet Change 110:26–39

Minder JR, Mote PW, Lundquist JD (2010) Surface temperature lapse rates over complex terrain: lessons from the Cascade Mountains. J Geophys Res 115:D14122, doi:10.1029/2009JD013493

Myers N, Mittermeier RA, Mittermeier CG, da Fonseca GA, Kent J (2000) Biodiversity hotspots for conservation priorities. Nature 403:853–858

Pauli H, Gottfried M, Reiter K, Klettner C, Grabherr G (2007) Signals of range expansions and contractions of vascular plants in the high Alps: observations (1994–2004) at the GLORIA* master site Schrankogel, Tyrol, Austria. Glob Change Biol 13:147–156

Pepin N, Losleben M (2002) Climate change in the Colorado Rocky Mountains: free air versus surface temperature trends. Int J Climatol 22:311–329

Pepin NC, Seidel DJ (2005) A global comparison of surface and free-air temperatures at high elevations. J Geophys Res 110:D03104, doi:10.1029/2004JD005047

Reuter HI, Nelson A, Jarvis A (2007) An evaluation of void-filling interpolation methods for SRTM data. Int J Geogr Inf Sci 21:983–1008

Shrestha AB, Wake CP, Mayewski PA, Dibb JE (1999) Maximum temperature trends in the Himalaya and its vicinity: an analysis based on temperature records from Nepal for the period 1971–94. J Clim 12:2775–2786

von Storch H, Zwiers FW (2001) Statistical analysis in climate research. Cambridge University Press, Cambridge

Wang A, Zeng X (2012) Evaluation of multireanalysis products with in situ observations over the Tibetan Plateau. J Geophys Res 117:D05102, doi:10.1029/2011JD016553

You Q, Kang S, Aguilar E, Yan Y (2008) Changes in daily climate extremes in the eastern and central Tibetan Plateau during 1961–2005. J Geophys Res 113:D07, doi:10.1029/2007JD009389

You Q, Kang S, Pepin N, Flügel WA, Sanchez-Lorenzo A, Yan Y, Zhang Y (2010a) Climate warming and associated changes in atmospheric circulation in the eastern and central Tibetan Plateau from a homogenized dataset. Global Planet Change 72:11–24

You Q, Kang S, Pepin N, Flügel WA, Yan Y, Behrawan H, Huang J (2010b) Relationship between temperature trend magnitude, elevation and mean temperature in the Tibetan Plateau from homogenized surface stations and reanalysis data. Global Planet Change 71:124–133

Yu H, Luedeling E, Xu J (2010) Winter and spring warming result in delayed spring phenology on the Tibetan Plateau. Proc Natl Acad Sci USA 107:22151–22156

Zhang Q, Xu CY, Tao H, Jiang T, Chen YD (2010) Climate changes and their impacts on water resources in the arid regions: a case study of the Tarim River basin, China. Stochastic Environ Res Risk Assess 24:349–358

Editorial responsibility: Oliver Frauenfeld, College Station, Texas, USA

Submitted: February 22, 2013; Accepted: September 8, 2013
Proofs received from author(s): December 17, 2013